

# Theoretical Study of Spin Observables in $pd$ Elastic Scattering at Energies $T_p = 800\text{--}1000$ MeV

M. N. Platonova\* and V. I. Kukulin†

*Skobeltsyn Institute of Nuclear Physics, Lomonosov Moscow State University, Moscow 119991, Russia*

(Dated: October 15, 2019)

Various spin observables (analyzing powers and spin-correlation parameters) in  $pd$  elastic scattering at  $T_p = 800\text{--}1000$  MeV are analyzed within the framework of the refined Glauber model. The theoretical model uses as input spin-dependent  $NN$  amplitudes obtained from the most recent partial-wave analysis and also takes into account the deuteron  $D$  wave and charge-exchange effects. Predictions of the refined Glauber model are compared with the existing experimental data. Reasonable agreement between the theoretical calculations and experimental data at low momentum transfers  $|t| \lesssim 0.2$  (GeV/ $c$ )<sup>2</sup> is found for all observables considered. Moderate discrepancies found in this region are shown to be likely due to uncertainties in the input  $NN$  amplitudes. Qualitative agreement at higher momentum transfers is also found for most observables except the tensor ones with mixed  $x$  and  $z$  polarization components. Possible reasons for observed deviations of the model calculations from the data at  $|t| > 0.2$  (GeV/ $c$ )<sup>2</sup> are discussed.

## I. INTRODUCTION

Proton-deuteron elastic scattering being the simplest nucleon-nucleus collision process is well suited for studying the basic properties of nuclear force. Due to small number of active particles,  $pd$  elastic scattering at intermediate energies is widely used for testing different theoretical models of  $2N$  and  $3N$  interaction, including non-standard mechanisms such as production of baryon and dibaryon resonances. While  $pd$  elastic scattering has been extensively studied experimentally and theoretically during more than 50 years, the new data are still being accumulated, thus extending the existing database and calling for suitable theoretical approaches for their interpretation.

A large portion of the new precise experimental data on intermediate-energy  $pd$  scattering (both elastic and inelastic) have come from the Cooler Synchrocyclotron at the Jülich FZ (COSY) (see the dedicated review [1]). One should mention here the very recent COSY-ANKE measurements of the small-angle  $dp$  elastic differential cross section at equivalent proton energies  $T_p$  around 900 MeV [2], the deuteron analyzing powers at  $T_p = 600$  and 1135 MeV [3], and the proton analyzing power in  $pd$  elastic scattering at  $T_p = 796$  MeV and five higher energies from 1600 to 2400 MeV [4]. Among the other recent data collected after 2010 are the RIKEN measurements of the deuteron analyzing powers at  $T_p = 250$  and 294 MeV [5, 6] and Dubna data on the small-angle differential cross section and deuteron vector analyzing power at  $T_p = 1000$  MeV [7], the large-angle differential cross section at  $T_p$  from 500 to 900 MeV [8, 9] and  $T_p = 1250$  MeV [10] and deuteron analyzing powers at  $T_p = 440$  MeV [11].

The  $pd$  and  $dp$  elastic scattering data at energies  $T_p <$

350 MeV can be analyzed theoretically by exact solution of the three-body Faddeev equations with a realistic  $NN$  potential as input [12]. The theoretical calculations strongly deviate from experiment at large scattering angles at  $T_p > 100$  MeV, and this deviation is generally attributed to the effect of  $3N$  forces [5, 6]. However inclusion of conventional  $3N$  forces based on production of intermediate  $\Delta$  isobar removes the observed discrepancies only partially. This is a deep puzzle intimately related to our poor understanding of the short-range mechanisms of  $NN$  and  $3N$  interaction.

At higher energies, the situation is even more unclear. On the one hand, numerous experiments (see, e.g., the works of Dubna and Saclay groups [13–19]) have revealed interesting structures in large-angle (in particular, backward)  $dp$  elastic scattering which indicate manifestation of the non-nucleon, i.e., isobar and possibly dibaryon, degrees of freedom (see also [20]). On the other hand, the existing high-precision  $NN$  potentials cannot be used in the region of  $T_p > 350$  MeV, and hence the solution of Faddeev equations becomes unreliable (and also too complicated). So, one does not possess an exact theoretical treatment of  $pd$  scattering in the GeV energy region even for two-body interactions and low momentum transfers. In this area, one generally applies the approximate multiple-scattering schemes, which usually take into account single and double scattering between the proton and nucleons in the deuteron and use  $NN$  amplitudes as input. The most famous one is the Glauber diffraction theory [21, 22] which is a high-energy and small-momentum transfer approximation to the exact multiple-scattering series. There are also several more sophisticated approaches (e.g., the relativistic multiple-scattering theory [23–25] or the more recent one [26, 27]), which include various corrections to the Glauber approximation (mainly due to off-shell and relativistic effects), however still restricted to single and double scattering. Hence, these theoretical schemes essentially account for the two lowest iterations of the Faddeev equations, with inclusion of relativistic effects and some additional mech-

\*Electronic address: [platonova@nucl-th.sinp.msu.ru](mailto:platonova@nucl-th.sinp.msu.ru)

†Electronic address: [kukulin@nucl-th.sinp.msu.ru](mailto:kukulin@nucl-th.sinp.msu.ru)

anisms important for large-angle scattering. While such approaches are much more involved than the Glauber diffraction theory, they should be applied carefully, bearing in mind that various corrections to the Glauber  $pd$  scattering amplitude tend to cancel each other, e.g., the off-shell part of the double-scattering term (omitted in the Glauber model) substantially cancels the contributions of higher order rescattering terms [28].

Thus, before considering any corrections to the Glauber theory, it is worth developing the most accurate theoretical model within the framework of the Glauber approximation, taking into account the recent progress in describing  $NN$  scattering and deuteron properties. That was the motivation of elaborating the refined Glauber model in Refs. [29, 30], which is essentially the conventional Glauber diffraction model extended to incorporate spin degrees of freedom. The refined version uses as input all ten helicity  $pp$  and  $np$  amplitudes obtained from the modern partial-wave analysis (PWA) of the George Washington University group (SAID) [31, 32] and employs the deuteron  $S$ - and  $D$ -wave functions derived in the high-precision  $NN$ -potential models (e.g., CD-Bonn [33]). The model also takes into account the process of double charge exchange, which is a manifestation of isospin dependence of the general  $NN$  amplitude. It should be noted that while the Glauber approach cannot help resolve the numerous discrepancies found in the large-angle  $pd$  scattering, it gives an accurate theoretical treatment of the small-angle region at intermediate energies. Thus, given the high precision of experimental data and reliable  $NN$  input, even the small deviations between the Glauber model calculations and experiment can be considered as indication of some non-trivial effects, related to  $3N$  forces and non-nucleon degrees of freedom.

The generalized scheme [29, 30] allowed for the first time to analyze within the diffraction model not only unpolarized cross sections, but also various spin-dependent observables, which are much more sensitive to the tiny details of  $pd$  interaction. In previous works [29, 30] we calculated the proton and deuteron analyzing powers at energies  $T_p = 250$  and  $440$  MeV and some of the deuteron analyzing powers at  $1000$  MeV and obtained very good agreement with existing experimental data at transferred momenta squared  $|t| < 0.3\text{--}0.4$  (GeV/ $c$ )<sup>2</sup>. For two lower energies, we also found surprisingly good agreement with the exact three-body calculations based on solution of the Faddeev equations in the same momentum-transfer region [29]. In the recent work [34] our formalism was applied to  $pd$  elastic scattering at  $T_p = 135$  and  $200$  MeV. A very good description of experimental data on differential cross sections, analyzing powers and some of the spin-correlation parameters was achieved at these energies, though at first glance  $T_p = 135$  MeV seems to be very low for application of the (high-energy) Glauber approach. The recent data on the vector and tensor deuteron analyzing powers in  $dp$  elastic scattering at the equivalent proton energies  $T_p = 600$  and  $1135$  MeV [3] were also

very well described by our model, with somewhat better agreement at higher energy. Besides that, the model was quite successfully applied to the antiproton-deuteron scattering at energies ranging from  $50$  to  $300$  MeV [35].

The very recent application of the refined Glauber model was the analysis of the new high-precision COSY-ANKE data [2] on the  $dp$  elastic differential cross section taken at  $T_p$  between  $882.2$  and  $918.3$  MeV in the transferred momentum range  $0.08 < |t| < 0.26$  (GeV/ $c$ )<sup>2</sup>. In these calculations, we used as input the recently updated  $NN$  PWA of the SAID group [36] which gives somewhat different  $NN$  amplitudes than the older solution [31] at  $T_p > 500$  MeV. Very good agreement between the theoretical calculation at  $T_p = 900$  MeV and experimental data was found at low momentum transfers  $|t| < 0.2$  (GeV/ $c$ )<sup>2</sup> [2]. At higher  $|t|$  values, the theoretical calculation was shown to significantly underestimate the data. Quite surprisingly, the range of applicability of the refined Glauber model turned out to be smaller than that found previously for lower energies (i.e.,  $|t| < 0.3\text{--}0.4$  (GeV/ $c$ )<sup>2</sup> at  $T_p = 250$  and  $440$  MeV) [29]. To establish the origin of this discrepancy, it is important to consider also the spin observables which can readily be calculated in the refined Glauber model at the same energies.

Unfortunately, the only new data on  $pd$  elastic spin observables in the energy range  $T_p = 800\text{--}1000$  MeV collected after 2010 are the above-mentioned data on the proton analyzing power [4] and on the deuteron vector analyzing power [7], the latter data having rather large uncertainties. On the other hand, there exist a rich set of older experimental data at  $T_p = 800$  MeV, including all proton and deuteron analyzing powers and a number of spin-correlation parameters and spin-transfer coefficients [37–45]. These numerous 800-MeV data have not yet been analyzed within the Glauber model.

Thus, the aim of this work is to study a large number of spin observables in  $pd$  elastic scattering at energies  $T_p = 800\text{--}1000$  MeV within the refined Glauber model and compare the results with existing experimental data. While previous works [3, 29, 30] dealt with some of the deuteron analyzing powers only (in the GeV energy region), here all proton and deuteron analyzing powers and also spin-correlation parameters are considered. This study will give a comprehensive test of the model and provide a theoretical basis for the future experiments on  $pd$  elastic spin observables at these and higher energies. Such experiments with polarized proton and deuteron beams are planned at, e.g., the NICA-SPD facility under construction at JINR (Dubna, Russia) [46].

The paper is organized as follows. In Sec. II we briefly outline the basic theoretical formalism. In Sec. III we present the results of the calculations and compare them with experimental data. In Sec. IV we discuss the origin of discrepancies found between the calculations and the data. We conclude in Sec. V. Some details on transformation of the amplitudes and observables between different notations are given in Appendix.

## II. THEORETICAL MODEL

The full formalism of the refined Glauber model was derived in Refs. [29, 30]. Here we briefly remind the basic formulas for amplitudes and give expressions for observables which were not considered previously.

The  $pd$  elastic scattering amplitude  $M$  in the Glauber model is the sum of the single- and double-scattering terms which are expressed through  $pp$  and  $pn$  amplitudes  $M_p$  and  $M_n$  and the deuteron wave function  $\Psi_d$ :

$$M(\mathbf{q}) = M^{(s)}(\mathbf{q}) + M^{(d)}(\mathbf{q}), \quad (1)$$

$$M^{(s)}(\mathbf{q}) = \int d^3r e^{i\mathbf{q}\cdot\mathbf{r}/2} \Psi_d(\mathbf{r}) [M_n(\mathbf{q}) + M_p(\mathbf{q})] \Psi_d(\mathbf{r}), \quad (2)$$

$$M^{(d)}(\mathbf{q}) = \frac{i}{4\pi^{3/2}} \int d^2q' \int d^3r e^{i\mathbf{q}'\cdot\mathbf{r}} \Psi_d(\mathbf{r}) [M_n(\mathbf{q}_2) M_p(\mathbf{q}_1) + M_p(\mathbf{q}_2) M_n(\mathbf{q}_1) - M_c(\mathbf{q}_2) M_c(\mathbf{q}_1)] \Psi_d(\mathbf{r}), \quad (3)$$

$\mathbf{q}$  being the overall 3-momentum transfer (so that  $t = -q^2$  in the center-of-mass system),  $\mathbf{q}_1 = \mathbf{q}/2 - \mathbf{q}'$  and  $\mathbf{q}_2 = \mathbf{q}/2 + \mathbf{q}'$  — the momenta transferred in collisions with individual target nucleons, and  $M_c(\mathbf{q}) = M_n(\mathbf{q}) - M_p(\mathbf{q})$  — the amplitude of the charge-exchange process  $pn \rightarrow np$ .

The amplitude  $M$  is expanded into 12 terms invariant under space and time reflections which are constructed from the scalar products of the unit vectors  $\hat{k} = (\mathbf{p} + \mathbf{p}')/|\mathbf{p} + \mathbf{p}'|$ ,  $\hat{q} = (\mathbf{p} - \mathbf{p}')/|\mathbf{p} - \mathbf{p}'|$ ,  $\hat{n} = \hat{k} \times \hat{q}$  forming the right-handed system ( $\mathbf{p}$  and  $\mathbf{p}'$  being the momenta of the incident and outgoing proton, respectively) and spin vectors of the proton ( $\frac{1}{2}\boldsymbol{\sigma}$ ) and deuteron ( $\mathbf{S}$ ). The coefficients of the expansion are the invariant amplitudes  $A_i(q)$ ,  $i = 1, \dots, 12$ , viz.

$$M[\mathbf{p}, \mathbf{q}; \boldsymbol{\sigma}, \mathbf{S}] = (A_1 + A_2 \boldsymbol{\sigma} \cdot \hat{n}) + (A_3 + A_4 \boldsymbol{\sigma} \cdot \hat{n})(\mathbf{S} \cdot \hat{q})^2 + (A_5 + A_6 \boldsymbol{\sigma} \cdot \hat{n})(\mathbf{S} \cdot \hat{n})^2 + A_7 \boldsymbol{\sigma} \cdot \hat{k} \mathbf{S} \cdot \hat{k} + A_8 \boldsymbol{\sigma} \cdot \hat{q} (\mathbf{S} \cdot \hat{q} \mathbf{S} \cdot \hat{n} + \mathbf{S} \cdot \hat{n} \mathbf{S} \cdot \hat{q}) + (A_9 + A_{10} \boldsymbol{\sigma} \cdot \hat{n}) \mathbf{S} \cdot \hat{n} + A_{11} \boldsymbol{\sigma} \cdot \hat{q} \mathbf{S} \cdot \hat{q} + A_{12} \boldsymbol{\sigma} \cdot \hat{k} (\mathbf{S} \cdot \hat{k} \mathbf{S} \cdot \hat{n} + \mathbf{S} \cdot \hat{n} \mathbf{S} \cdot \hat{k}). \quad (4)$$

Analogously, the  $pp$  and  $pn$  amplitudes  $M_N$  ( $N = p, n$ ) are expanded into six terms:

$$M_N[\mathbf{p}, \mathbf{q}; \boldsymbol{\sigma}, \boldsymbol{\sigma}_N] = A_N + C_N \boldsymbol{\sigma} \cdot \hat{n} + C'_N \boldsymbol{\sigma}_N \cdot \hat{n} + B_N \boldsymbol{\sigma} \cdot \hat{k} \boldsymbol{\sigma}_N \cdot \hat{k} + (G_N + H_N) \boldsymbol{\sigma} \cdot \hat{q} \boldsymbol{\sigma}_N \cdot \hat{q} + (G_N - H_N) \boldsymbol{\sigma} \cdot \hat{n} \boldsymbol{\sigma}_N \cdot \hat{n}, \quad (5)$$

where  $\boldsymbol{\sigma}$  and  $\boldsymbol{\sigma}_N$  are the Pauli matrices corresponding to the incident and target nucleons. For the double-scattering term, the unit vectors  $\hat{k}, \hat{q}, \hat{n}$  are defined separately for each individual  $NN$  collision.

Following the initial approach of Franco and Glauber [22], we define the  $pd$  as well as  $NN$  amplitudes in the laboratory frame, where scattering off nucleon and deuteron can be easily related to each other.

Thus, we distinguish the amplitudes  $C_N$  and  $C'_N$  which, for small scattering angles, are interrelated as  $C'_N \approx C_N + i(q/2m_N)A_N$  [47].<sup>1</sup> One should however bear in mind that the unit vectors  $\hat{k}$  and  $\hat{q}$  which are orthogonal in the center-of-mass frame, are approximately orthogonal in the laboratory frame at small scattering angles, where  $p \approx p'$ . Assuming  $p = p'$  and, consequently,  $-t = q^2$  in the laboratory frame is consistent with the fixed-scatterer approximation inherent to the Glauber theory.<sup>2</sup> The neglect of the deuteron recoil energy is justified when it is small compared to the momentum transfer, i.e., when  $q^2/4m_d^2 \ll 1$ .

The final formulae for all  $pd$  amplitudes  $A_1$ – $A_{12}$  expressed in terms of the  $NN$  amplitudes  $A_N, B_N, C_N, C'_N, G_N$  and  $H_N$  ( $N = n, p$ ) and the deuteron monopole and quadrupole form factors are to be found in Refs. [29, 30]. In the present calculations, we used the  $NN$  amplitudes corresponding to the recent SAID PWA solution SM16 [32, 36] and the high-precision CD-Bonn deuteron wave function [33]. Both the  $NN$  amplitudes and the deuteron wave function were parameterized as sums of five Gaussian terms as described in Refs. [29, 30].

We complete this section with the definitions for  $pd$  elastic observables. The differential cross section is related to the amplitude  $M$  as

$$d\sigma/dt = \frac{1}{6} \text{Sp} (MM^+). \quad (6)$$

The general polarization observable is defined as (see, e.g., [42])

$$C(\alpha, \beta, \gamma, \delta) = \frac{\text{Sp} (M\sigma_\alpha S_\beta M^+ \sigma_\gamma S_\delta)}{\text{Sp} (MM^+)}, \quad (7)$$

where  $\alpha = \{x, y, z\}$  and  $\gamma = \{x', y', z'\}$  correspond to the polarization of the initial and final proton, while  $\beta = \{x, y, z, xx, yy, zz, xy, zy, xz\}$  and  $\delta = \{x', y', z', x'x', y'y', z'z', x'y', z'y', x'z'\}$  — to the (vector or tensor) polarization of the initial and final deuteron. For the tensor values of  $\beta \equiv \beta_1\beta_2$  ( $\beta_1, \beta_2 = \{x, y, z\}$ ),  $S_\beta$  means the quadrupole operator  $S_{\beta_1\beta_2} = \frac{3}{2}(S_{\beta_1} S_{\beta_2} + S_{\beta_2} S_{\beta_1}) - 2\delta_{\beta_1\beta_2}$  (the same holds for the index  $\delta$ ). Each of the four indices  $\alpha, \beta, \gamma, \delta$  can also be zero, which means that the respective particle has no definite polarization.

In this paper we deal with the observables corresponding to the polarized initial particles, i.e., beam and target. These are the proton (vector) analyzing powers

<sup>1</sup> Note the inverted sign of the amplitudes  $C_N$  and  $C'_N$  compared to that in Ref. [47], due to a different definition of the unit vector  $\hat{n}$ . Note also that the imaginary unit was missed in the last term of Eq. (14) in Ref. [29].

<sup>2</sup> One should note that the above relations are valid for arbitrary  $q$  not only in the center-of-mass, but also in the Breit frame which is convenient to use for describing  $pd$  (as well as  $ed$ ) scattering when going beyond the fixed-scatterer approximation. At small transferred momenta, the Breit frame almost coincides with the laboratory frame.

$A_\alpha^p \equiv C(\alpha, 0, 0, 0)$ , the deuteron vector and tensor analyzing powers  $A_\alpha^d \equiv C(0, \alpha, 0, 0)$  and  $A_\beta \equiv C(0, \beta, 0, 0)$  for  $\beta = \beta_1\beta_2$ , and the vector and tensor spin-correlation parameters  $C_{\alpha,\beta} \equiv C(\alpha, \beta, 0, 0)$ , all with non-zero values of  $\alpha$  and  $\beta$ .<sup>3</sup>

If to define the coordinate system  $xyz = \{\hat{q}\hat{n}\hat{k}\}$ , the  $pd$  elastic observables can be readily expressed in terms of the invariant amplitudes  $A_1$ – $A_{12}$  (see Eq. (4)). The explicit formulas for the differential cross section and all vector and tensor analyzing powers were presented in Refs. [29, 30].<sup>4</sup> Here we add the formulas for non-vanishing vector and tensor spin-correlation parameters:

$$\begin{aligned}
C_{y,y} &= 2 \operatorname{Re}[(2A_1^* + A_3^* + 2A_5^*)A_{10} \\
&\quad + (2A_2^* + A_4^* + 2A_6^*)A_9 - A_7^*A_{11} - A_8^*A_{12}]/\Sigma, \\
C_{x,x} &= 2 \operatorname{Re}[(2A_1^* + 2A_3^* + A_5^*)A_{11} - A_6^*A_{12} \\
&\quad - A_7^*A_{10} + A_8^*A_9]/\Sigma, \\
C_{z,x} &= 2 \operatorname{Im}[(2A_2^* + 2A_4^* + A_6^*)A_{11} - A_5^*A_{12} \\
&\quad + A_7^*A_9 - A_8^*A_{10}]/\Sigma, \\
C_{x,z} &= -2 \operatorname{Im}[(2A_2^* + A_4^* + A_6^*)A_7 + (A_3^* - A_5^*)A_8 \\
&\quad - A_9^*A_{11} + A_{10}^*A_{12}]/\Sigma, \\
C_{z,z} &= 2 \operatorname{Re}[(2A_1^* + A_3^* + A_5^*)A_7 + (A_4^* - A_6^*)A_8 \\
&\quad - A_{10}^*A_{11} + A_9^*A_{12}]/\Sigma, \\
C_{y,yy} &= 2 \operatorname{Re}[A_1^*(2A_6 - A_4) + A_3^*(A_6 - A_2 - A_4) \\
&\quad + A_5^*(2A_2 + A_4 + 2A_6) - 3A_7^*A_8 + 2A_9^*A_{10} \\
&\quad - 3A_{11}^*A_{12}]/\Sigma, \\
C_{y,xx} &= 2 \operatorname{Re}[A_1^*(2A_4 - A_6) + A_3^*(2A_2 + 2A_4 + A_6) \\
&\quad + A_5^*(A_4 - A_2 - A_6) + 3A_7^*A_8 - A_9^*A_{10}]/\Sigma, \\
C_{y,xz} &= -3 \operatorname{Im}[A_3^*A_{10} + A_4^*A_9 + A_7^*A_{11} + A_8^*A_{12}]/\Sigma, \\
C_{y,zz} &= -C_{y,yy} - C_{y,xx}, \\
C_{x,xy} &= 3 \operatorname{Re}[(2A_1^* + A_3^* + A_5^*)A_8 + (A_4^* - A_6^*)A_7 \\
&\quad + A_9^*A_{11} - A_{10}^*A_{12}]/\Sigma, \\
C_{z,xy} &= 3 \operatorname{Im}[(2A_2^* + A_4^* + A_6^*)A_8 + (A_3^* - A_5^*)A_7 \\
&\quad - A_9^*A_{12} + A_{10}^*A_{11}]/\Sigma, \\
C_{x,zy} &= -3 \operatorname{Im}[(2A_2^* + 2A_4^* + A_6^*)A_{12} - A_5^*A_{11} \\
&\quad + A_8^*A_9 - A_7^*A_{10}]/\Sigma, \\
C_{z,zy} &= 3 \operatorname{Re}[(2A_1^* + 2A_3^* + A_5^*)A_{12} - A_6^*A_{11} \\
&\quad + A_7^*A_9 - A_8^*A_{10}]/\Sigma, \tag{8}
\end{aligned}$$

<sup>3</sup> All observables of the type  $C(\alpha, \beta, 0, 0)$  are sometimes denoted in literature as  $A_{\alpha\beta}$  (see, e.g., [39]); in this case, spin-correlation parameters are called correlated analyzing powers, though this notation is far less common.

<sup>4</sup> Note that the “ $\cdot$ ” sign of  $A_{xz}$  was accidentally dropped in Eq. 4 of Refs. [29] and [30].

where

$$\begin{aligned}
\Sigma &= 3 d\sigma/dt = 3(|A_1|^2 + |A_2|^2) + 2\left(\sum_{i=3}^{12} |A_i|^2\right) \\
&\quad + \operatorname{Re}[2A_1^*(A_3 + A_5) + 2A_2^*(A_4 + A_6) \\
&\quad + A_3^*A_5 + A_4^*A_6]. \tag{9}
\end{aligned}$$

To compare our model calculations with experimental data, we have to transform all  $pd$  observables to the Madison frame which is conventionally used in experiments, i.e.,  $xyz = \{\hat{S}\hat{N}\hat{L}\}$ , where  $\hat{L} = \hat{p}$ ,  $\hat{N} = \widehat{p \times p'}$ , and  $\hat{S} = \hat{N} \times \hat{L}$ .<sup>5</sup> In fact, the  $pd$  invariant amplitudes can be defined directly in the Madison frame as was done in Ref. [34]. However, we prefer to use the advantages of the  $\{\hat{q}\hat{n}\hat{k}\}$  coordinate system conventional for the Glauber model calculations. The symmetry between the initial and final states allows to easily apply  $T$ -invariance which leads to the 12 independent amplitudes, rather than 18 dependent ones which have to be dealt with in the Madison frame. The observables obtained in terms of these 12 amplitudes can then be readily transformed to any other coordinate system.

The Madison frame is related to the  $\{\hat{q}\hat{n}\hat{k}\}$  system by the rotation in the scattering plane ( $xz$ ) by the half scattering angle  $\theta/2$ , and the reflection of the normal ( $y$ ) axis, viz.

$$\hat{S} = -a\hat{q} + b\hat{k}, \quad \hat{N} = -\hat{n}, \quad \hat{L} = b\hat{q} + a\hat{k}, \tag{10}$$

where  $a = \cos(\theta/2)$ ,  $b = \sin(\theta/2)$ . So, the transformed observables involving just the  $y$ -axis will only change their sign ( $A_y^p$ ,  $A_y^d$  and  $C_{y,yy}$ ) or even remain unchanged ( $A_{yy}$  and  $C_{y,y}$ ). Other observables containing  $x$  and/or  $z$  indices would slightly change their behavior at small scattering angles. The explicit transformation rules for the observables considered here are given in Appendix.

### III. RESULTS

The results of the refined Glauber model calculations for  $pd$  elastic differential cross section and various spin observables at the proton energies  $T_p = 800, 900$  and  $1000$  MeV are presented in Figs. 1–5. Our theoretical predictions are compared with the experimental data available in this energy region.<sup>6</sup> There are numerous data on the unpolarized differential cross section [2, 7, 37, 38, 48–51], the proton analyzing power [4, 37–40], deuteron

<sup>5</sup> A lot of measurements were actually performed on  $dp$  rather than  $pd$  scattering. The Madison frame for  $dp$  scattering is related to that for  $pd$  scattering by reflection of two axes  $x \rightarrow -x$ ,  $z \rightarrow -z$ , which does not affect the definition of observables.

<sup>6</sup> The available data include also  $dp$  elastic scattering measurements at the incident deuteron energies which are twice the proton energies considered here.

analyzing powers [7, 41, 42], spin-correlation parameters [39, 42–44] and spin-transfer coefficients [39, 40, 42–45]. Most of these data were taken at  $T_p = 800$  MeV. We plot here our results for the differential cross section and 11 spin observables (out of 22 needed for a complete experiment) measured in a broad range of momentum transfers (including the low-momentum transfer region), i.e., the proton and deuteron vector analyzing powers, three deuteron tensor analyzing powers and six (out of 12) spin-correlation parameters — two vector and four tensor ones — measured in [42]. All polarization observables are plotted in the Madison frame (see Sec. II and Appendix).

Our results for the differential cross section in comparison with the existing experimental data at  $T_p = 800$ –1000 MeV are presented in Fig. 1. The contribution of single scattering is also shown by thin lines.<sup>7</sup> As is seen from the figure (see also Ref. [2]), the refined Glauber model calculations accurately describe the experimental database at low momentum transfers<sup>8</sup>  $|t| \leq 0.2$  (GeV/c)<sup>2</sup> and then begin to deviate from the data, though remaining in the qualitative agreement with them in the forward hemisphere. It is also clearly seen from Fig. 1 that the energy dependence (the increasing slope) of the calculated cross section as a function of  $|t|$ , which arises mainly from the similar energy dependence of the input  $NN$  cross sections, is almost negligible at  $|t| \leq 0.2$  (GeV/c)<sup>2</sup> but becomes clearly visible at higher  $|t|$ . So, in the region where the Glauber model describes the data, the cross section is almost energy-independent at  $T_p = 800$ –1000 MeV, and this is confirmed by the existing data. However, a more accurate theoretical model should be used to study the energy dependence of the  $pd$  cross section at higher momentum transfers.

The results for the vector and tensor analyzing powers are shown in Figs. 2 and 3. Here we see again reasonable (though not perfect) agreement with the data at  $|t| \leq 0.2$  (GeV/c)<sup>2</sup>. Some deviations from the data found in this region are likely to be related to the uncertainties in the input  $NN$  amplitudes (see the discussion in Sec. IV A). One should also bear in mind the uncertainties present in the  $pd$  data. Thus, if to compare two datasets [41] and [42] for the deuteron analyzing powers at  $T_p = 800$  MeV (see Figs. 2 and 3), it is seen that the latter data are described a bit better by our model cal-

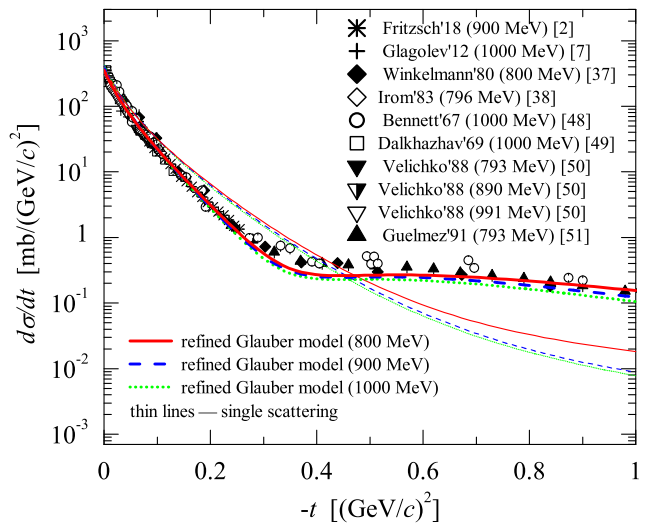


FIG. 1: (Color online) Differential cross sections of  $pd$  elastic scattering at the incident (equivalent) proton energies  $T_p = 800$ –1000 MeV. Solid (red), dashed (blue) and dotted (green) lines show the refined Glauber model calculations at  $T_p = 800$ , 900 and 1000 MeV, respectively, with the input  $NN$  amplitudes corresponding to the SAID PWA solution SM16 [32, 36]. Thin lines of the same type (color) show the single-scattering contribution only. Theoretical calculations are compared with the existing experimental database at  $T_p = 793$ –1000 MeV [2, 7, 37, 38, 48–51].

culations. In fact, these data were obtained by the same group as [41] and thus appear to be more precise, though still having some uncertainty in the beam polarization. Further, it is quite surprising that the proton analyzing power  $A_y^p$  at  $|t| \leq 0.3$  (GeV/c)<sup>2</sup> is reproduced better at low energies (440, 250 and even 135 MeV [29, 34]) than in the GeV region, though the applicability of the Glauber theory should improve with energy. The situation here is similar but even more drastic as for the differential cross section, and the reason probably lies in the uncertainties of the input  $NN$  amplitudes rising with energy. In this connection, it would be very instructive to study the behavior of  $A_y^p$  at  $T_p \geq 1$  GeV theoretically, especially in view of the recently published data [4] at  $T_p$  from 1600 to 2400 MeV. Unfortunately, these data cannot be presently analyzed by the refined Glauber model, due to absence of the reliable  $np$  PWA at energies  $T_p > 1300$  MeV [36].

Figs. 2 and 3 also show at least qualitative (or even semiquantitative) agreement between the Glauber theory and experiment at  $|t| > 0.2$  (GeV/c)<sup>2</sup> for all vector and tensor analyzing powers, except for the tensor one  $A_{xz}$ , which is poorly reproduced at  $0.2 < |t| < 0.4$  (GeV/c)<sup>2</sup>. While the experimental  $A_{xz}$  has a pronounced dip in this region, the refined Glauber model calculations give the smooth curve very close to zero. In fact, this  $|t|$  region includes the transition between the dominance of the single- and double-scattering terms, which is very sensitive to the tiny details of the  $pd$  scattering process, and especially to the deuteron  $D$ -wave contribution (or,

<sup>7</sup> The single-scattering contribution is plotted in Figs. 1–5 up to  $|t| = 1$  (GeV/c)<sup>2</sup>, though the Gaussian parametrization [29] used in calculations reproduces  $NN$  helicity amplitudes only for  $q \leq 0.7$  GeV/c ( $|t| \leq 0.5$  (GeV/c)<sup>2</sup>) and may deviate from them at higher momentum transfers. Nevertheless,  $pd$  elastic scattering at  $|t| > 0.35$  (GeV/c)<sup>2</sup> is dominated by the double-scattering term, which contains  $NN$  amplitudes in the vicinity of  $|t|/4$ , so, the results of the full calculations correspond to the correct  $NN$  input until  $|t| = 1$  (GeV/c)<sup>2</sup> and higher.

<sup>8</sup> Here and further on we do not consider the region  $0 \leq |t| \lesssim 0.04$  (GeV/c)<sup>2</sup> where Coulomb effects neglected in our model calculations are significant in  $pd$  scattering.

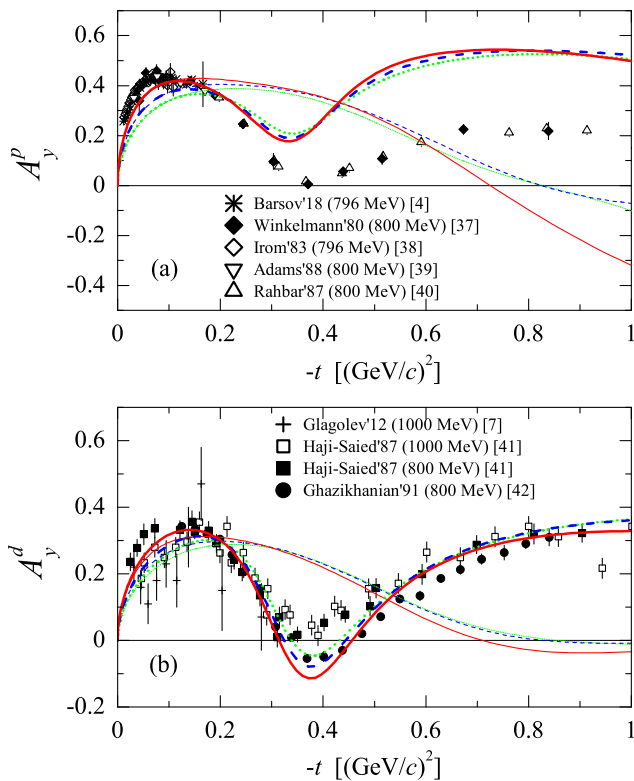


FIG. 2: (Color online) Proton (a) and deuteron (b) vector analyzing powers in  $pd$  ( $dp$ ) elastic scattering at the incident (equivalent) proton energies  $T_p = 800$ – $1000$  MeV. The meaning of lines is the same as in Fig. 1. Experimental data are taken from Refs. [4, 7, 37–42].

more precisely, to the quadrupole deuteron form factor containing the interference between the  $S$ - and  $D$ -wave components). So, the tensor analyzing power  $A_{xz}$  appears to be highly sensitive to an accurate description of the terms associated with the deuteron quadrupole form factor (see the discussion in Sec. IV B).

The situation with the vector and tensor spin-correlation parameters is quite similar to that with the analyzing powers. As is seen from Figs. 4 and 5, all considered spin-correlation parameters are described quite well at low momentum transfers  $|t| \leq 0.2$   $(\text{GeV}/c)^2$ , and most of them are described at least qualitatively at higher momentum transfers up to  $|t| = 1$   $(\text{GeV}/c)^2$ . Only the tensor spin-correlation parameter  $C_{y,xz}$  which behaves similarly to the tensor analyzing power  $A_{xz}$  is poorly reproduced in the region  $0.2 < |t| < 0.5$   $(\text{GeV}/c)^2$ , likely for the same reason as  $A_{xz}$ . Unfortunately, the most problematic observables with the mixed  $x$  and  $z$  polarization components are also those having the largest experimental uncertainties. So, to get a more clear picture of their theoretical description, it would be highly desirable to measure these observables with better statistics.

We further turn to the analysis of energy dependence found for  $pd$  spin observables in the region  $T_p = 800$ –

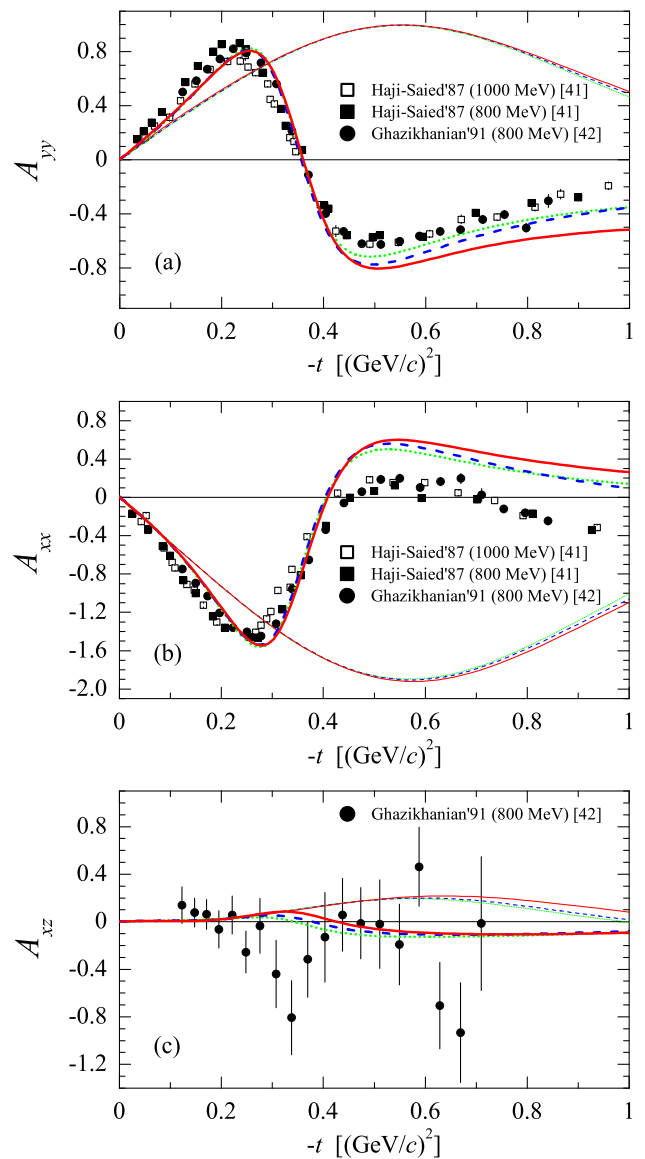


FIG. 3: (Color online) Deuteron tensor analyzing powers in  $dp$  elastic scattering at the equivalent proton energies  $T_p = 800$ – $1000$  MeV. The meaning of lines is the same as in Fig. 1. Experimental data are taken from Refs. [41, 42].

$1000$  MeV. As is seen from Figs. 2–5, our calculations reveal some energy dependence of the vector analyzing powers at low momentum transfers, where the difference between the results at  $T_p = 800$  and  $1000$  MeV is up to 25%. This theoretical prediction is qualitatively confirmed by the experimental data [41] for  $A_y^d$  shown in Fig. 2. Quite similar but weaker energy dependence was found for the vector spin-correlation parameters. On the other hand, the tensor analyzing powers and tensor spin-correlation parameters, except for  $C_{z,xy}$ , were found to be almost independent of energy at  $|t|$ . Since the energy dependence of observables calculated within the refined Glauber model comes mainly from the similar de-

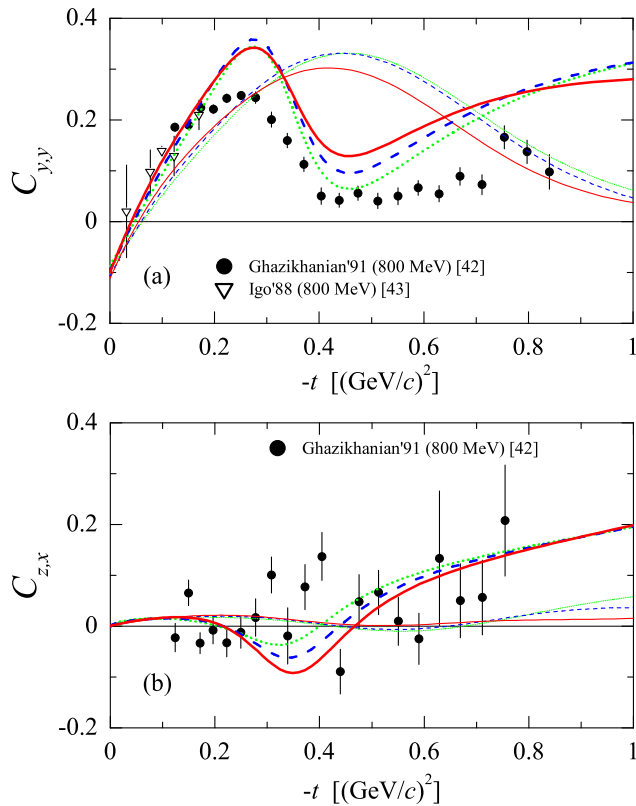


FIG. 4: (Color online) Vector spin-correlation parameters in  $pd$  ( $dp$ ) elastic scattering at the incident (equivalent) proton energies  $T_p = 800$ – $1000$  MeV. The meaning of lines is the same as in Fig. 1. Experimental data are taken from Refs. [42, 43].

pendence of the input  $NN$  amplitudes, the energy independence is quite expectable for the tensor observables which are mostly sensitive to the deuteron wave function. On the other hand, the spin-correlation parameter  $C_{z,xy}$  which was found to be strongly energy dependent at low momentum transfers provides a crucial test for the input  $NN$  amplitudes and their treatment in the model for  $pd$  elastic scattering.

#### IV. DISCUSSION

##### A. Sensitivity of the low-momentum-transfer $pd$ observables to the input $NN$ amplitudes

Influence of the  $NN$  input on the results obtained within the refined Glauber model for  $pd$  observables is worth to be discussed in detail.

First, we studied the deviations between the different SAID PWA solutions by comparing the results for  $pd$  differential cross section and spin observables at  $T_p = 1$  GeV obtained with the use of three  $NN$  PWA solutions: two recent solutions SM16 (unweighted) and

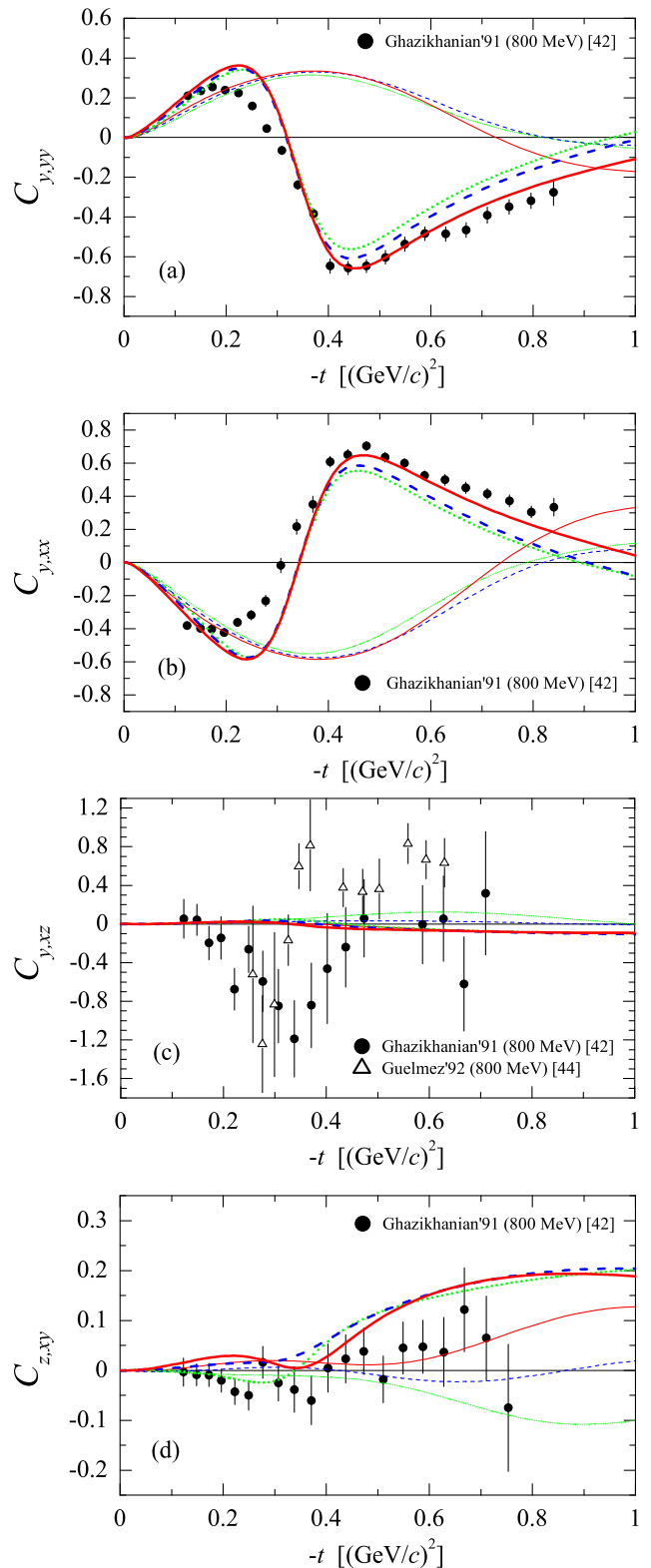


FIG. 5: (Color online) Tensor spin-correlation parameters in  $pd$  ( $dp$ ) elastic scattering at the incident (equivalent) proton energies  $T_p = 800$ – $1000$  MeV. The meaning of lines is the same as in Fig. 1. Experimental data are taken from Refs. [42, 44].

WF16 (weighted) [36] and an older one SP07 [31] used in our previous works [29, 30]. The difference between these three solutions is almost negligible at  $T_p \leq 500$  MeV, but becomes visible at  $T_p \simeq 1$  GeV [36]. We found that the predictions based on different PWA solutions are almost indistinguishable at low momentum transfers  $|t| \leq 0.2$  (GeV/c)<sup>2</sup> and begin to slightly diverge at higher  $|t|$ . However this divergence is considerably smaller than the discrepancies between the theoretical results and experimental data at  $|t| > 0.2$  (GeV/c)<sup>2</sup>. So, while it is natural to choose the most recent (unweighted) solution SM16 [36] for the Glauber model calculations, any one out of the three above PWA solutions may be used.

Second, though the SAID PWA is considered to be reliable in the region  $T_p \leq 1$  GeV, there are some discrepancies between the energy-dependent solutions and  $NN$  experimental data. For instance, we found an underestimation of the recent high-precision  $A_y^p$  data in  $pp$  scattering at  $T_p = 796$  MeV [52] by all SAID PWA solutions starting from SP07 [32], which at small scattering angles (corresponding to  $|t| \simeq 0.05$  (GeV/c)<sup>2</sup>) amounts to 5–7%. Some underestimation takes place also for the recent  $pn$   $A_y^p$  data [4], though there are much less data-points than in the  $pp$   $A_y^p$  measurement [52]. This deviation between the SAID PWA solutions and  $pN$   $A_y^p$  data apparently leads to some underestimation of the  $pd$   $A_y^p$  and  $A_y^d$  data at small  $|t|$  in our model calculations. Indeed, in small-angle  $pd$  scattering at intermediate energies  $A_y^d$  is approximately proportional to  $A_y^p$  (with a coefficient of 2/3) [53], and  $A_y^p$  is in turn approximately equal to the average  $A_y^p$  in  $pp$  and  $np$  scattering [54].

To test the impact of the input  $NN$  amplitudes on the small-angle behavior of  $pd$  observables, we tried to find a modification of the SAID  $NN$  amplitudes which could simultaneously improve the description of both  $NN$  and  $pd$  observables at small momentum transfers. Since the analyzing powers in  $pN$  scattering  $A_y^p = -2\text{Re}[(A_N^* + G_N^* - H_N^*)C_N]/(d\sigma_N/dt)$  (with the sign given for the Madison frame) are mostly sensitive to the interference between the central  $A_N$  and spin-orbit  $C_N$  amplitudes, we tried to fit the existing  $pN$   $A_y^p$  data at  $|t| < 0.5$  (GeV/c)<sup>2</sup> by adjusting the spin-orbit amplitudes  $C_p$  and  $C_n$ . Simultaneously, we fitted the existing data on  $pN$  differential cross sections  $d\sigma_N/dt$  and spin-correlation parameters  $A_{yy} = 2\text{Re}[A_N^*(G_N - H_N) - B_N^*(G_N + H_N) + |C_N|^2]/(d\sigma_N/dt)$  to fix the moduli of the amplitudes  $C_N$  and also the  $pn$  charge-exchange cross section (which contains  $|C_n - C_p|^2$ ) to fix their relative phase. We also included in the fit the data on  $A_y^p$  in  $pd$  scattering.

As a result, we found a modification of the spin-orbit  $NN$  amplitudes (shown in Fig. 6) that improves significantly the description of small-angle  $pp$   $A_y^p$  data (see Fig. 7) without worsening the description of other  $NN$  data included in the fit, compared to the SAID SM16 solution. As is clearly seen from Fig. 8, the same modification allows for a significantly better description of both proton and deuteron analyzing powers in  $pd$  elastic scattering within the refined Glauber model, whereas

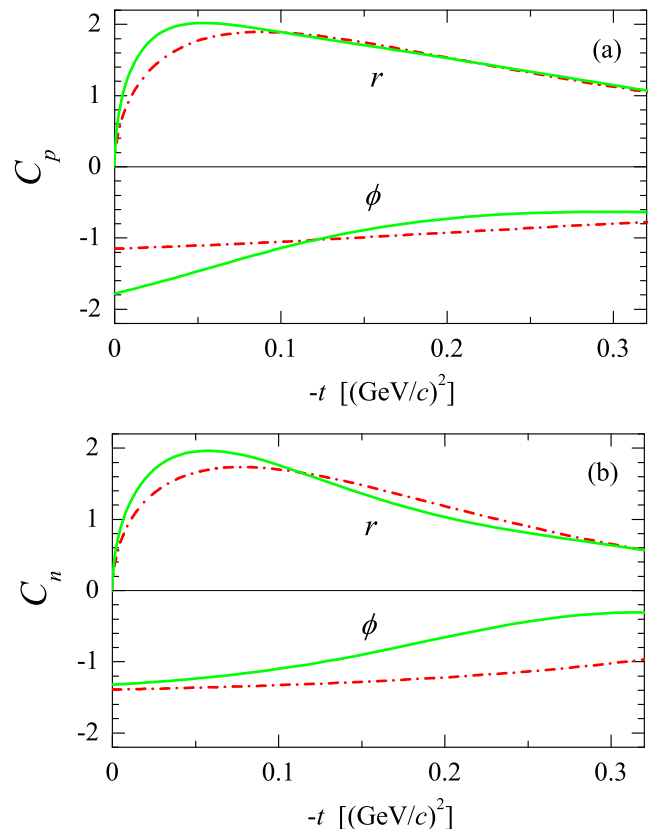


FIG. 6: (Color online) Amplitudes  $C_p$  (a) and  $C_n$  (b) for  $pp$  and  $pn$  elastic scattering at  $T_p = 800$  MeV, respectively (see Eq. (5)), presented in the form  $re^{i\phi}$ . Upper lines on each figure show the moduli  $r$  [ $\sqrt{\text{mb}}/\text{GeV}$ ], and lower lines show the phases  $\phi$  [rad.] of the amplitudes. Dash-dotted (red) lines correspond to the SAID PWA solution SM16 [32, 36], while solid (green) lines show the modified  $NN$  amplitudes which allow for a better description of  $NN$  and  $pd$  observables simultaneously (see text).

their ratio remains almost unchanged due to its weak sensitivity to the spin-orbit  $NN$  amplitudes [53]. Simultaneously, we achieve better agreement with the data for the vector spin-correlation parameter  $C_{y,y}$  and, what is very important, for the tensor spin-correlation parameter  $C_{z,xy}$ , which is extremely sensitive to the input  $NN$  amplitudes, in the region  $|t| < 0.3$  (GeV/c)<sup>2</sup> (see Fig. 8). Other  $pd$  observables considered here are reproduced at the same level of accuracy as with initial (SAID SM16)  $NN$  amplitudes.

We also found some other discrepancies between the recent SAID PWA solutions and  $NN$  data (e.g., a 10% overestimation of the  $pn$  forward and backward (charge-exchange) cross sections) which could not be removed by any modification of the spin-orbit  $pn$  amplitude. Removing all these discrepancies requires a thorough revision of the SAID PWA which is not our task here. We have just shown the possibility to improve the description of small-angle  $pd$  observables in the refined Glauber model



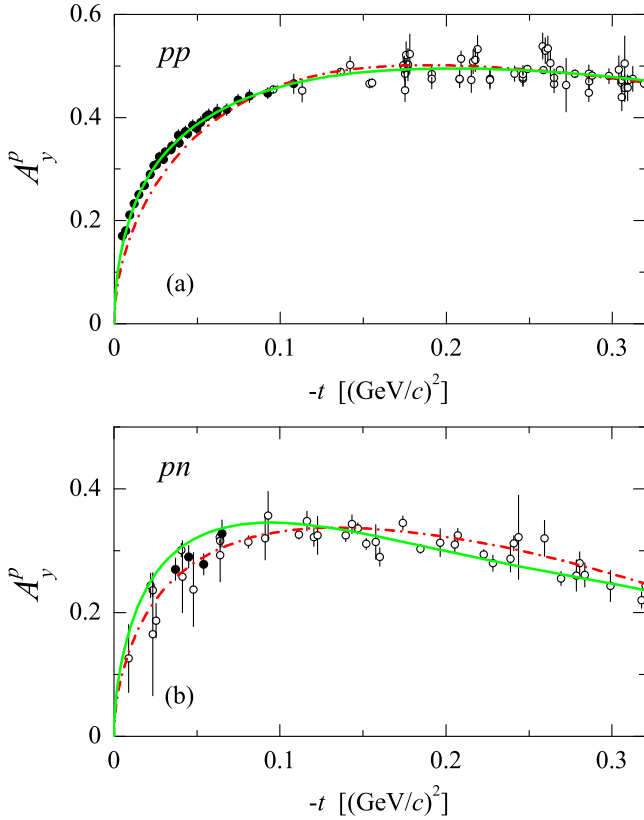


FIG. 7: (Color online) Analyzing power  $A_y^p$  in  $pp$  (a) and  $pn$  (b) elastic scattering at  $T_p = 800$  MeV. Dash-dotted (red) lines correspond to the SAID PWA solution SM16 [32, 36], while solid (green) lines show calculations with modified  $NN$  amplitudes  $C_p$  and  $C_n$  (see Fig. 6). Filled circles show the recent ANKE-COSY experimental data at  $T_p = 796$  MeV from Refs. [52] ( $pp$ ) and [4] ( $pn$ ), and open circles show other (older) data at  $T_p = 790$ –810 MeV from the SAID database [32].

by adjusting the input  $NN$  amplitudes consistently with  $NN$  experimental data. This result suggests that the remaining discrepancies for  $pd$  observables at  $|t| < 0.3$   $(\text{GeV}/c)^2$  could be removed by further refinement of the  $NN$  input.

The ambiguity of the input  $NN$  amplitudes obtained from the PWA in the GeV energy region is apparently related to experimental uncertainties in the  $NN$  data which affect the PWA solutions. While the uncertainties in the  $pp$  or  $pn$  amplitudes can in principle be traced in the  $NN$  experimental data, their estimation is much more nontrivial for the sum of  $pp$  and  $pn$  amplitudes entering the single-scattering term of the Glauber  $pd$  amplitude, and even more complicated for the bilinear combinations of  $NN$  amplitudes entering the double-scattering term. These problems with  $NN$  amplitudes might as well be the reason for the better description of  $pd$  observables at 135 and 250 MeV than in the GeV region [29, 34], since under (and slightly above) the pion production threshold the exact unitarity imposes more rigorous constraints on

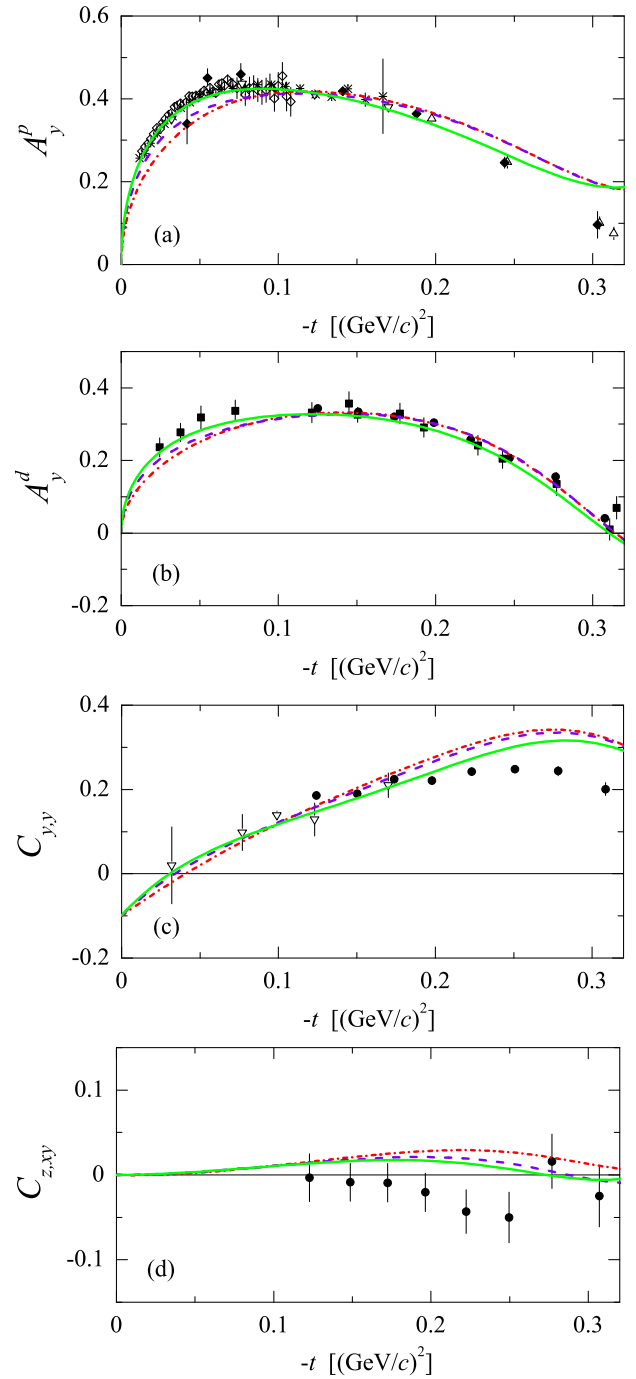


FIG. 8: (Color online) Proton analyzing power  $A_y^p$  (a), deuteron analyzing power  $A_y^d$  (b) and vector spin-correlation parameter  $C_{y,y}$  (c) in  $pd$  ( $dp$ ) elastic scattering at the incident (equivalent) proton energy  $T_p = 800$  MeV. Dash-dotted (red), dashed (violet) and solid (green) lines show the refined Glauber model calculations with  $NN$  amplitudes corresponding to the SAID PWA solution SM16 [32, 36], with the modified amplitude  $C_p$  and with modified amplitudes  $C_p$  and  $C_n$  (see Fig. 6), respectively. Experimental data at  $T_p = 796$  and 800 MeV are the same as in Figs. 2, 4 and 5.

the  $NN$  amplitudes obtained by PWA.

At the same time, we were unable to find a modification of  $NN$  amplitudes consistent with  $NN$  data that could significantly reduce the discrepancies between our model calculations and  $pd$  data at  $|t| \geq 0.3$  (GeV/c)<sup>2</sup>. So, the main reason for these discrepancies is to be sought in the limitations of the Glauber model and missing dynamical contributions.

### B. Possible reasons for discrepancies at higher momentum transfers

In this subsection we discuss possible reasons for the failure of the refined Glauber model in description of  $pd$  elastic observables at  $|t| > 0.2$ – $0.3$  (GeV/c)<sup>2</sup>. The gradually rising deviation between the data and theoretical calculations which are seen for the most  $pd$  observables are quite expectable in view of the decreasing validity of the Glauber approach with momentum transfer. On the other hand, the severe discrepancies have been found for the tensor analyzing power  $A_{xz}$  and spin-correlation parameter  $C_{y,xz}$  in the single-to-double scattering transition region ( $0.2 < |t| < 0.5$  (GeV/c)<sup>2</sup>), which is very sensitive to the deuteron  $D$ -wave contribution. These discrepancies appear to be not just the consequence of the low-momentum approximation. It should be noted here that terms which connect the deuteron  $D$ -wave with the product of two spin-dependent  $NN$  amplitudes were neglected in the double-scattering amplitude of our model [29, 30]. This approximation was justified by the relative smallness of the spin-dependent  $NN$  amplitudes in comparison to the large spin-independent ones in the GeV energy region. Though this assumption becomes less accurate as the momentum transfer increases, it still works well in the double-scattering amplitude where  $NN$  amplitudes enter in the vicinity of  $|t|/4$ . So, the small omitted terms can hardly give a sizeable contribution to the observables in the considered momentum transfer region.

The more detailed analysis shows that the dominant contribution to  $pd$  elastic scattering at GeV energies and small momentum transfers  $|t| < 0.2$  (GeV/c)<sup>2</sup> comes from the largest invariant amplitude  $A_1$ . At higher momentum transfers, the amplitudes  $A_3$  (which dominates at  $0.3 < |t| < 0.55$  (GeV/c)<sup>2</sup>) and  $A_5$  also become significant (see Fig. 9). Other nine invariant amplitudes are considerably smaller than  $A_1$  at all momentum transfers. In fact, all three above amplitudes include sizeable terms associated with the deuteron quadrupole form factor, but these terms in  $A_3$  and  $A_5$  have an opposite sign as compared to that in  $A_1$  (see Table II in Ref. [29]). Hence, they substantially cancel each other in such observables as  $A_y^d$  and  $A_{yy}$  which contain the combination  $2A_1 + A_3 + 2A_5$ , but not in  $A_{xz}$  which contains a large contribution from  $A_3$  not compensated by  $A_1$  (see Eq. (4) in Ref. [29]). So,  $A_{xz}$  should be more sensitive to an accurate description of the terms related to the deuteron quadrupole form fac-

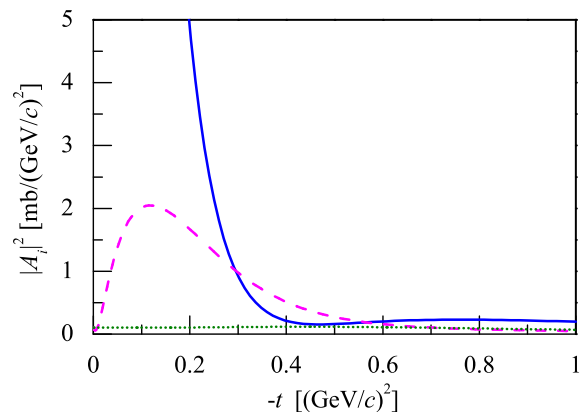


FIG. 9: (Color online) Moduli squared of the  $pd$  elastic scattering amplitudes  $A_1$  (solid line),  $A_3$  (dashed line) and  $A_5$  (dotted line) at  $T_p = 800$  MeV calculated within the refined Glauber model.

tor, than other analyzing powers. Quite similar conclusions could be drawn also for the tensor spin-correlation parameter  $C_{y,xz}$ .

It should be emphasized that the problem with description of the tensor  $pd$  observables appear to be tightly connected to a long-standing problem with the deuteron quadrupole moment. In fact, its experimental value is  $Q^{\text{exp}} = 0.2859(3)$  fm<sup>2</sup>, while the high-precision  $NN$  potentials predict a bit lower values  $Q^{\text{theor}} \simeq 0.270$ – $0.280$  fm<sup>2</sup> [33]. This small (2–6%) discrepancy seems from first glance to be not very serious. However it is likely related to the inaccuracy in short-range behavior of the deuteron  $D$ -wave function where the error may be large if to take into account the low probability of the  $D$ -wave component in the deuteron. Thus this inaccuracy in the short-range deuteron  $D$  wave will translate to errors for the tensor observables, such as  $A_{xz}$  and  $C_{z,xy}$ . Hence, it would be very instructive to study the sensitivity of these observables at  $0.2 < |t| < 0.5$  (GeV/c)<sup>2</sup> to the behavior of the deuteron  $D$ -wave short-range component. This however should be done beyond the on-shell approximation for the double-scattering term, which prevents the proper account of the short-range deuteron structure in the Glauber theory.

On the other hand, the observed discrepancies might be related to some dynamical mechanisms of the short-range nature, which were included neither in the Glauber model nor in the more sophisticated multiple-scattering approaches. In fact, even the fully spin-dependent relativistic multiple-scattering theory [24] with parameters of the off-shell  $NN$  amplitudes adjusted to fit the whole  $pd$  elastic database at 800 MeV was unable to describe satisfactory the above tensor observables [42]. So, one of the possible candidates for the missing dynamical mechanisms is some kind of  $3N$  forces. While the conventional  $3N$  force based on the intermediate  $\Delta$  excitation was shown to contribute predominantly to the large-angle  $pd$

scattering [5, 6], the non-conventional three-body force which arise from the meson exchange between the incident proton and the deuteron as a whole (i.e., the six-quark, or dibaryon, component of the deuteron) [55] might give some sizeable corrections to the multiple-scattering amplitude in the forward hemisphere [56]. Such a  $3N$  force is tightly interrelated with the short-range  $S$ - and  $D$ -wave components of the deuteron wave function, and it has also a strong spin-orbit term, which can affect the description of polarization observables sensitive to the spin-orbit interactions (such as  $A_y^p$ ). These interesting questions certainly deserve further investigation and will be considered in our future work.

## V. SUMMARY

In this work we presented comparison between the predictions for the differential cross section and various spin observables in  $pd$  elastic scattering in the GeV energy region given by the refined Glauber model (with full account of spin degrees of freedom) and experimental data. As an input in our model calculations, fully realistic  $NN$  helicity amplitudes obtained from the most recent PWA (SAID) and the accurate deuteron  $S$ - and  $D$ -wave functions derived within the high-precision  $NN$  potential model (CD-Bonn) were employed. While in our previous works [29, 30] only three deuteron analyzing powers at  $T_p = 1$  GeV were considered, in this paper 11 polarization observables including all five analyzing powers and six spin-correlation parameters at proton energies  $T_p = 800, 900$  and  $1000$  MeV have been calculated, thus providing a more complete picture.

As is clearly seen from Figs. 1–5, our results are in quite reasonable agreement with available experimental data at transferred momenta squared  $|t| \lesssim 0.2$  (GeV/ $c$ )<sup>2</sup> for all observables considered. Some deviations from the data found in this region are likely to be due to uncertainties in the input  $NN$  amplitudes arising from experimental uncertainties of  $NN$  elastic scattering data and ambiguities in the PWA procedure above the pion production threshold. In fact, we were able to remove some discrepancies between the SAID PWA solutions and  $NN$  data at  $T_p = 800$  MeV and simultaneously improve the description of a number of  $pd$  spin observables at  $|t| < 0.3$  (GeV/ $c$ )<sup>2</sup> by adjusting the spin-orbit  $NN$  amplitudes. Though good agreement with the data at small momentum transfers is generally expectable for the Glauber theory, it has been achieved here for the first time for a large number of highly sensitive spin observables, thus providing a reliable theoretical basis for the future experiments with polarized proton and deuteron beams, which are planned, e.g., at the NICA-SPD facility at JINR, Dubna. Since the same formalism is straightforwardly applicable for the  $\bar{p}d$  scattering, it can also serve as a tool for analysis of the future experiments with polarized antiproton beams, which are planned, e.g., within the FAIR project in GSI Darmstadt.

Though the description of the data by our model calculations clearly worsens with rising momentum transfer, we found at least qualitative agreement between theory and experiment for the most observables considered at  $|t|$  up to 1 (GeV/ $c$ )<sup>2</sup>. Remarkably, the strongest deviations from the data were found in the region  $0.2 < |t| < 0.5$  (GeV/ $c$ )<sup>2</sup> which includes the transition between the dominance of single and double scattering. The  $pd$  elastic observables (especially the tensor ones with mixed  $x$  and  $z$  polarization components) in this region are highly sensitive to the deuteron quadrupole form factor. So, the origin of the observed discrepancies should be sought in improper treatment of the deuteron  $D$ -wave component at short distances and in probable contributions from the missing dynamical mechanisms associated with the short-range structure of the deuteron. A good candidate for such a mechanism is the proton scattering from the deuteron as a whole, i.e., from the short-range (dibaryon) component of the deuteron. In this case, one deals with the novel type of three-body force [55, 56], the contribution of which to  $pd$  scattering should rise with momentum transfer.

Since the validity of the Glauber model is restricted by the momentum transfer, the angular range of its applicability becomes larger at lower energies. This explains the very good agreement between the refined Glauber model calculations and experiment for the  $pd$  elastic cross section and spin observables at  $T_p = 135$  MeV till  $\theta_{c.m.} \simeq 80$  deg. [34], while in the GeV region the data are described well till  $\theta_{c.m.} \simeq 30$  deg. only.

The present study, along with earlier works, proves the refined Glauber model to be a very useful tool for describing scattering of fast protons off deuterons (and, in general, fast hadrons off loosely-bound nuclei) at low momentum transfers  $|t| \lesssim 0.2\text{--}0.3$  (GeV/ $c$ )<sup>2</sup> in a wide range of intermediate energies (at least  $T_p = 135\text{--}1135$  MeV). In this region, the exact multiple-scattering series may be represented by the Glauber amplitude based solely on the on-shell two-body interactions, without need for solution of very complicated three-body equations. However, the more accurate theoretical treatment is needed at higher momentum transfers. It would also be highly desirable to obtain more precise data for  $pd$  elastic spin observables with mixed  $x$  and  $z$  polarization components, which presently have very large experimental uncertainties.

## Acknowledgments

The authors appreciate fruitful discussions with Colin Wilkin, who carefully read the initial version of the manuscript and made valuable comments and suggestions. The work was supported by the Russian Foundation for Basic Research, grants Nos. 19-02-00014 and 19-02-00011, and the Foundation for the Advancement of Theoretical Physics and Mathematics “BASIS”.

- [1] C. Wilkin, *Eur. Phys. J.* **A53**, 114 (2017), 1611.07250.
- [2] C. Fritzscht et al., *Phys. Lett.* **B784**, 277 (2018), 1805.12499.
- [3] D. Mchedlishvili et al., *Nucl. Phys.* **A977**, 14 (2018), 1805.05778.
- [4] S. Barsov et al., *Eur. Phys. J.* **A54**, 225 (2018), 1808.01792.
- [5] K. Sekiguchi et al., *Phys. Rev. C* **83**, 061001 (2011), 1106.0180.
- [6] K. Sekiguchi et al., *Phys. Rev. C* **89**, 064007 (2014).
- [7] V. V. Glagolev, V. P. Ladygin, N. B. Ladygina, and A. A. Terekhin, *Eur. Phys. J.* **A48**, 182 (2012).
- [8] A. Terekhin et al., *EPJ Web Conf.* **138**, 03012 (2017).
- [9] A. A. Terekhin et al., *Phys. Atom. Nucl.* **80**, 1061 (2017), [*Yad. Fiz.* **80**, 594 (2017)].
- [10] P. K. Kurilkin et al. (HADES), *PoS Baldin-ISHEPP-XXI*, 040 (2012).
- [11] P. K. Kurilkin et al., *Phys. Lett.* **B715**, 61 (2012), 1207.3509.
- [12] W. Glöckle, H. Witala, D. Huber, H. Kamada, and J. Golak, *Phys. Rept.* **274**, 107 (1996).
- [13] V. I. Komarov, G. E. Kosarev, G. P. Reshetnikov, and O. V. Savchenko, *Yad. Fiz.* **16**, 234 (1972).
- [14] L. S. Azhgirei et al., *Phys. Lett.* **B391**, 22 (1997).
- [15] L. S. Azhgirei et al., *Phys. Atom. Nucl.* **61**, 432 (1998), [*Yad. Fiz.* **61**, 494 (1998)].
- [16] V. Punjabi et al., *Phys. Lett.* **B350**, 178 (1995).
- [17] J. Arvieux et al., *Phys. Rev. Lett.* **50**, 19 (1983).
- [18] J. Arvieux et al., *Nucl. Phys.* **A431**, 613 (1984).
- [19] P. Berthet et al., *J. Phys. G* **8**, L111 (1982).
- [20] Yu. N. Uzikov, *Phys. Part. Nucl.* **29**, 583 (1998), [*Fiz. Elem. Chast. Atom. Yadra* **29**, 1405 (1998)].
- [21] R. J. Glauber, *Phys. Rev.* **100**, 242 (1955).
- [22] V. Franco and R. J. Glauber, *Phys. Rev.* **142**, 1195 (1966).
- [23] G. Alberi, M. Bleszynski, and T. Jaroszewicz, *Ann. Phys.* **142**, 299 (1982).
- [24] E. Bleszynski, M. Bleszynski, and T. Jaroszewicz, *AIP Conf. Proc.* **150**, 1208 (1986).
- [25] E. Bleszynski, M. Bleszynski, and T. Jaroszewicz, *Phys. Rev. Lett.* **59**, 423 (1987).
- [26] N. B. Ladygina, *Phys. Atom. Nucl.* **71**, 2039 (2008), 0705.3149.
- [27] N. B. Ladygina, *Eur. Phys. J.* **A42**, 91 (2009), 0906.1910.
- [28] D. R. Harrington, *Phys. Rev.* **184**, 1745 (1969).
- [29] M. N. Platonova and V. I. Kukulkin, *Phys. Rev. C* **81**, 014004 (2010), [Erratum: *Phys. Rev. C* **94**, 069902(E) (2016)], 1612.08694.
- [30] M. N. Platonova and V. I. Kukulkin, *Phys. Atom. Nucl.* **73**, 86 (2010), [*Yad. Fiz.* **73**, 90 (2010)].
- [31] R. A. Arndt, W. J. Briscoe, I. I. Strakovsky, and R. L. Workman, *Phys. Rev. C* **76**, 025209 (2007), 0706.2195.
- [32] The SAID partial-wave analysis website (2018), URL <http://gwdac.phys.gwu.edu>.
- [33] R. Machleidt, *Phys. Rev. C* **63**, 024001 (2001), nucl-th/0006014.
- [34] A. A. Temerbayev and Yu. N. Uzikov, *Phys. Atom. Nucl.* **78**, 35 (2015), [*Yad. Fiz.* **78**, 38 (2015)].
- [35] Yu. N. Uzikov and J. Haidenbauer, *Phys. Rev. C* **87**, 054003 (2013).
- [36] R. L. Workman, W. J. Briscoe, and I. I. Strakovsky, *Phys. Rev. C* **94**, 065203 (2016), 1609.01741.
- [37] E. Winkelmann et al., *Phys. Rev. C* **21**, 2535 (1980).
- [38] F. Irom, G. J. Igo, J. B. McClelland, C. A. Whitten, and M. Bleszynski, *Phys. Rev. C* **28**, 2380 (1983).
- [39] D. L. Adams et al., *Nucl. Phys.* **A480**, 530 (1988).
- [40] A. Rahbar et al., *Phys. Lett.* **B194**, 338 (1987).
- [41] M. Haji-Saied et al., *Phys. Rev. C* **36**, 2010 (1987).
- [42] V. Ghazikhanian et al., *Phys. Rev. C* **43**, 1532 (1991).
- [43] G. Igo et al., *Phys. Rev. C* **38**, 2777 (1988).
- [44] E. Guelmez et al., *Phys. Rev. C* **45**, 22 (1992).
- [45] T.-H. Sun et al., *Phys. Rev.* **C31**, 515 (1985).
- [46] A. Guskov (SPD Working Group), in *8th International Conference on Quarks and Nuclear Physics (QNP2018) Tsukuba, Japan, November 13–17, 2018* (2019), 1904.04779.
- [47] C. Sorensen, *Phys. Rev. D* **19**, 1444 (1979).
- [48] G. W. Bennett et al., *Phys. Rev. Lett.* **19**, 387 (1967).
- [49] N. Dalkhazhav et al., *Sov. J. Nucl. Phys.* **8**, 196 (1969), [*Yad. Fiz.* **8**, 342 (1968)].
- [50] G. N. Velichko et al., *Sov. J. Nucl. Phys.* **47**, 755 (1988), [*Yad. Fiz.* **47**, 1185 (1988)].
- [51] E. Guelmez et al., *Phys. Rev. C* **43**, 2067 (1991).
- [52] Z. Bagdasarian et al., *Phys. Lett.* **B739**, 152 (2014), 1409.8445.
- [53] Yu. Uzikov and C. Wilkin, *Phys. Lett.* **B793**, 224 (2019), 1902.03596.
- [54] C. Wilkin, private communication.
- [55] V. I. Kukulkin, V. N. Pomerantsev, M. Kaskulov, and A. Faessler, *J. Phys.* **G30**, 287 (2004), nucl-th/0308059.
- [56] M. N. Platonova and V. I. Kukulkin, *J. Phys. Conf. Ser.* **381**, 012110 (2012).

### Appendix: Transformation of polarization observables in $pd$ elastic scattering to the Madison frame

In this Appendix we give the explicit formulas which should be applied to transform the  $pd$  elastic spin observables from the  $xyz = \{\hat{q}\hat{n}\hat{k}\}$  frame used in deriving the formalism of the refined Glauber model to the  $xyz = \{\hat{S}\hat{N}\hat{L}\}$  (Madison) frame conventionally used in experiments (see definitions in Sec. II).

There are the expressions for analyzing powers:

$$\begin{aligned}
 A_y^{p(\text{Mad})} &= -A_y^p, & A_y^{d(\text{Mad})} &= -A_y^d, \\
 A_{yy}^{(\text{Mad})} &= A_{yy}, \\
 A_{xx}^{(\text{Mad})} &= \frac{1}{2}(1 + \cos\theta) A_{xx} + \frac{1}{2}(1 - \cos\theta) A_{zz} \\
 &\quad - \sin\theta A_{xz}, \\
 A_{xz}^{(\text{Mad})} &= -\cos\theta A_{xz} - \frac{1}{2}\sin\theta (A_{xx} - A_{zz}), \\
 A_{zz}^{(\text{Mad})} &= -A_{yy}^{(\text{Mad})} - A_{xx}^{(\text{Mad})}, \tag{A.1}
 \end{aligned}$$

and for spin-correlation parameters:

$$\begin{aligned}
C_{y,y}^{(\text{Mad})} &= C_{y,y}, \\
C_{x,x}^{(\text{Mad})} &= \frac{1}{2}(1 + \cos\theta) C_{x,x} + \frac{1}{2}(1 - \cos\theta) C_{z,z} \\
&\quad - \frac{1}{2}\sin\theta (C_{z,x} + C_{x,z}), \\
C_{z,x}^{(\text{Mad})} &= -\frac{1}{2}(1 + \cos\theta) C_{z,x} + \frac{1}{2}(1 - \cos\theta) C_{x,z} \\
&\quad - \frac{1}{2}\sin\theta (C_{x,x} - C_{z,z}), \\
C_{x,z}^{(\text{Mad})} &= -\frac{1}{2}(1 + \cos\theta) C_{x,z} + \frac{1}{2}(1 - \cos\theta) C_{z,x} \\
&\quad - \frac{1}{2}\sin\theta (C_{x,x} - C_{z,z}), \\
C_{z,z}^{(\text{Mad})} &= \frac{1}{2}(1 + \cos\theta) C_{z,z} + \frac{1}{2}(1 - \cos\theta) C_{x,x} \\
&\quad + \frac{1}{2}\sin\theta (C_{x,z} + C_{z,x}), \\
C_{y,yy}^{(\text{Mad})} &= -C_{y,yy}, \\
C_{y,xx}^{(\text{Mad})} &= -\frac{1}{2}(1 + \cos\theta) C_{y,xx} - \frac{1}{2}(1 - \cos\theta) C_{y,zz} \\
&\quad + \sin\theta C_{y,xz}, \\
C_{y,xz}^{(\text{Mad})} &= \cos\theta C_{y,xz} + \frac{1}{2}\sin\theta (C_{y,xx} - C_{y,zz}), \\
C_{y,zz}^{(\text{Mad})} &= -C_{y,yy}^{(\text{Mad})} - C_{y,xx}^{(\text{Mad})}, \\
C_{x,xy}^{(\text{Mad})} &= -\frac{1}{2}(1 + \cos\theta) C_{x,xy} - \frac{1}{2}(1 - \cos\theta) C_{z,zy} \\
&\quad + \frac{1}{2}\sin\theta (C_{z,xy} + C_{x,zy}), \\
C_{z,xy}^{(\text{Mad})} &= \frac{1}{2}(1 + \cos\theta) C_{z,xy} - \frac{1}{2}(1 - \cos\theta) C_{x,zy} \\
&\quad + \frac{1}{2}\sin\theta (C_{x,xy} - C_{z,zy}), \\
C_{x,zy}^{(\text{Mad})} &= \frac{1}{2}(1 + \cos\theta) C_{x,zy} - \frac{1}{2}(1 - \cos\theta) C_{z,xy} \\
&\quad + \frac{1}{2}\sin\theta (C_{x,xy} - C_{z,zy}), \\
C_{z,zy}^{(\text{Mad})} &= -\frac{1}{2}(1 + \cos\theta) C_{z,zy} - \frac{1}{2}(1 - \cos\theta) C_{x,xy} \\
&\quad - \frac{1}{2}\sin\theta (C_{z,xy} + C_{x,zy}). \tag{A.2}
\end{aligned}$$

We should note here that we did not transform the analyzing powers to the Madison frame in the previous works [29, 30]. However, when compared the theoretical predictions to experimental data, we inverted the sign of vector analyzing powers  $A_y^p$  and  $A_y^d$ . We also consid-

ered tensor analyzing powers  $A_{yy}$  (which is the same in both coordinate frames) and  $A_{xx}$  (which is changed only slightly by Eq. (A.1) in the forward hemisphere), so that, there was no significant error in comparing these observables to those measured in the Madison frame. The only analyzing power that changes its behavior substantially under the transformation (A.1) is  $A_{xz}$  (due to an admixture of large  $A_{xx}$ ), which was not considered in our previous works.

The expressions for some of the above observables in terms of 18  $pd$  amplitudes derived directly in the Madison frame and the relations of these amplitudes to our ones  $A_1$ – $A_{12}$  are to be found in Ref. [34].

We also give here an alternative representation of the  $pd$  elastic scattering amplitude in the  $\{\hat{q}\hat{n}\hat{k}\}$  frame, which has a more symmetric form than Eq. (4):

$$\begin{aligned}
M[\mathbf{p}, \mathbf{q}; \boldsymbol{\sigma}, \mathbf{S}] &= (M_1 + M_2 \boldsymbol{\sigma} \cdot \hat{n})(1 - (\mathbf{S} \cdot \hat{q})^2) \\
&\quad + (M_3 + M_4 \boldsymbol{\sigma} \cdot \hat{n})(1 - (\mathbf{S} \cdot \hat{n})^2) \\
&\quad + (M_5 + M_6 \boldsymbol{\sigma} \cdot \hat{n})(1 - (\mathbf{S} \cdot \hat{k})^2) \\
&\quad + iM_7 \boldsymbol{\sigma} \cdot \hat{k} \mathbf{S} \cdot \hat{k} \\
&\quad - M_8 \boldsymbol{\sigma} \cdot \hat{q} (\mathbf{S} \cdot \hat{q} \mathbf{S} \cdot \hat{n} + \mathbf{S} \cdot \hat{n} \mathbf{S} \cdot \hat{q}) \\
&\quad - i(M_9 + M_{10} \boldsymbol{\sigma} \cdot \hat{n}) \mathbf{S} \cdot \hat{n} + iM_{11} \boldsymbol{\sigma} \cdot \hat{q} \mathbf{S} \cdot \hat{q} \\
&\quad - M_{12} \boldsymbol{\sigma} \cdot \hat{k} (\mathbf{S} \cdot \hat{k} \mathbf{S} \cdot \hat{n} + \mathbf{S} \cdot \hat{n} \mathbf{S} \cdot \hat{k}). \tag{A.3}
\end{aligned}$$

The set of invariant amplitudes  $M_1$ – $M_{12}$  (multiplied by a standard normalization factor  $8p\sqrt{\pi s}$ ) was used in, e.g., Ref. [20] (note however that the direction of the unit vector  $\hat{n}$  was chosen there opposite to ours). These amplitudes are related to our ones  $A_1$ – $A_{12}$  as follows:

$$\begin{aligned}
A_1 &= M_1 + M_3 - M_5, & A_2 &= M_2 + M_4 - M_6, \\
A_3 &= M_5 - M_1, & A_4 &= M_6 - M_2, \\
A_5 &= M_5 - M_3, & A_6 &= M_6 - M_4, \\
A_7 &= iM_7, & A_8 &= -M_8, & A_9 &= -iM_9, \\
A_{10} &= -iM_{10}, & A_{11} &= iM_{11}, & A_{12} &= -M_{12}. \tag{A.4}
\end{aligned}$$

The  $pd$  elastic observables expressed in terms of the amplitudes  $M_1$ – $M_{12}$  look simpler than those given by Eq. (4) of Ref. [29] and Eq. (8) of the present paper. In particular, interference between different amplitudes vanishes in the expression for the differential cross section. On the other hand, such a representation is less transparent in sense that there are three large amplitudes  $M_1$ ,  $M_3$  and  $M_5$  instead of only one dominant amplitude  $A_1$  at low momentum transfers.